Characterization of lymph node optical properties for phantom fabrication

Veronica C. Torres, Todd Wilson, Chengyue Li, Lagnojita Sinha, Jovan G. Brankov, et al.

Veronica C. Torres, Todd Wilson, Chengyue Li, Lagnojita Sinha, Jovan G. Brankov, Kenneth M. Tichauer, "Characterization of lymph node optical properties for phantom fabrication," Proc. SPIE 10868, Advanced Biomedical and Clinical Diagnostic and Surgical Guidance Systems XVII, 1086813 (26 February 2019); doi: 10.1117/12.2513245

SPIE.

Event: SPIE BiOS, 2019, San Francisco, California, United States

Characterization of lymph node optical properties for phantom fabrication

Veronica C. Torres*[a], Todd Wilson[a], Chengyue Li[a], Lagnojita Sinha [a], Jovan G. Brankov[b], Kenneth M. Tichauer[a]
[a]Department of Biomedical Engineering, Illinois Institute of Technology, 3255 S Dearborn St., Chicago, IL USA 60616; [b]Department of Electrical and Computer Engineering, Illinois Institute of Technology, 3255 S Dearborn St., Chicago, IL USA 60616

ABSTRACT

Sentinel lymph node biopsy is a primary mean of staging cancer; however, the time-intensive nature of standard pathology limits the volume of the node that can be assessed. As a result, micrometastases can be missed, which have been shown to affect treatment decisions and therefore clinical outcomes. Optical imaging offers a potential solution for improved sensitivity and larger tissue evaluation, but an understanding of optical properties is necessary because of the high scattering nature of biological tissue. Here, time-domain optical imaging and measures of transmittance are used to characterize the optical properties of porcine lymph nodes at 685 nm and 780 nm. Results demonstrated values comparable to that of other soft biological tissue (685 nm: $\mu_a = 0.09 \pm 0.01 cm^{-1}$, $\mu_s' = 2.60 \pm 0.42\ cm^{-1}$, $g = 0.95$; 780 nm: $\mu_a = 0.24 \pm 0.10 cm^{-1}$, $\mu_s' = 3.35 \pm 0.14\ cm^{-1}$, $g = 0.92$). Based on these coefficients, optical properties of TiO_2 were investigated so that a protocol to fabricate a lymph node tissue-mimicking phantom could be defined.

Keywords: lymph node, optical properties, time domain, phantom

1. INTRODUCTION

The lymphatic system plays a vital role in breast, melanoma, and head and neck cancer as it serves as the primary route for cancer spread. Since the majority of all cancer-related deaths are caused by metastases, lymph node assessment, and specifically sentinel lymph node biopsy (SLNB) is a key step in staging.[1-3] Despite its prognostic importance, pathology of SLNB tissue still has high rates of false negatives. The standard protocol evaluates only ~1% of the entire lymph node volume because it is so time consuming, and the result is 30-60% of micrometastases going undetected.[4] Therefore, a more sensitive approach is needed.

While alternate methods that can improve sensitivity such as rapid cytokeratin immunohistochemistry[5], one-step nucleic acid amplification[6], and flow cytometry[7] exist, they still fail to sample the whole lymph node and/or result in destruction of the tissue such that subsequent pathology cannot be done.[8] Optical imaging provides a favorable potential solution because it can be low-cost, free of ionizing radiation and non-invasive. However, one stipulation of this approach is that the quality of imaging depends strongly on the optical properties of the sample. For instance, in the near-infrared (NIR) range where imaging of biological tissue is commonly done, absorption is low, but scattering dominates, thereby limiting resolution.[9] Thus, to account for this, it is important to have an understanding of these properties. With respect to instrumentation, scatter-rejection can be achieved via time- or angular-domain imaging to improve resolution, however there is a trade-off between resolution and signal that is dependent on the properties of the specimen.[10] Techniques including fluorescence laminar optical tomography[11] and mesoscopic fluorescence molecular tomography[12] rely on Monte Carlo simulation and accurate modeling of photon propagation through tissue. Furthermore, physical phantoms require an understanding of optical properties to calibrate and test the limits of instruments.[13]

Many biological tissues, both human and animal have been investigated in the NIR window;[14] however, to our knowledge, only one study exists that looks specifically at lymph nodes (Scolaro *et. al*)[15], which was done using optical coherence tomography (OCT) and therefore at 1320 nm. In this work, the optical properties (absorption coefficient μ_a, reduced scattering coefficient μ_s', attenuation coefficient μ_t, and anisotropy factor g) of porcine lymph nodes are characterized via time-domain optical imaging at 685 nm and 780 nm. Dilutions of scattering agents were then explored to identify methods of fabricating physical phantoms with optical properties to match that of actual

Advanced Biomedical and Clinical Diagnostic and Surgical Guidance Systems XVII
edited by Anita Mahadevan-Jansen, Warren S. Grundfest, Proc. of SPIE Vol. 10868
1086813 · © 2019 SPIE · CCC code: 1605-7422/19/$18 · doi: 10.1117/12.2513245

lymph nodes. With an understanding of these properties, the values can be applied to improve instrumentation, within simulation, and to create tissue-mimicking phantoms.

2. METHODS

2.1 Absorption coefficient and reduced scattering coefficient estimation

Estimation of the absorption coefficient, μ_a, and reduced scattering coefficient, μ_s', was done using measures of time-resolved transmittance. Thick tissue samples were used so that the diffusion approximation to the radiative transfer equation could be assumed to sufficiently model the temporal spreading of light as it passed through the medium.[16] This theory was expressed as follows:

$$\phi(t) = \phi_0(t) * at^{-\frac{3}{2}} \exp\left(-\frac{3(\mu_a+\mu_s')d^2}{4vt} - \mu_a vt\right), \quad (1)$$

where $\phi(t)$ is the temporal point spread function (TPSF), $\phi_0(t)$ is the instrument response function (IRF) of the system, $*$ denotes convolution, a is a scaling factor and fitting parameter, d is the sample thickness, and v represents the speed of light in the medium (typical soft tissue index of refraction, n = 1.4 was assumed[14]). Using Eq. (1), the coefficients μ_a and μ_s' were estimated with a least squares optimization code in MATLAB (Mathworks, Natick, MA). The TPSF and IRF were measured using an in-house made time-domain optical imaging system.[17] Illumination was sourced from a 685 nm picosecond laser diode (LDH- D-C-690, PicoQuant, Berlin, Germany) and 780 nm femtosecond pulsed laser (Medocino, Calmar Laser, Palo Alto, CA), and time-domain signal was collected with a single photon avalanche diode detector (PDM, Micro Photon Devices, Italy) synced to a time correlated single photon counting module (HydraHarp, PicoQuant). The transit time distribution of photons was measured at a resolution of 4 ± 12 ps.

First, for validation of the method described above, optical property estimation was conducted on a 3x3x4.8 cm^3 tissue-mimicking phantom block (Biomimic, INO, Quebec, Canada) with known properties (μ_a = 0.05 cm^{-1}, μ_s' = 10 cm^{-1}, g = 0.62, n = 1.51). Then, to estimate μ_a and μ_s' of lymph node tissue, enough lymph nodes to tightly fill a 4x4-cm^2 clear square glass container were surgically extracted from neck tissue of freshly slaughtered pigs (supplied by a local butcher). Each of the samples were placed in the imaging field of the system and the temporal pulse spread of the laser after passing through the medium was collected for both 685 nm and 780 nm wavelengths.

2.2 Anisotropy coefficient estimation

The scattering anisotropy factor, g, was estimated using thin tissue samples so that the condition of single scattering could be assumed and the Beer-Lambert law applied. The transmission of light was modeled as:

$$I = I_0 \exp(-\mu_t d), \quad (2)$$

where I is the transmitted power measured after passing through the sample, I_0 is the incident power, μ_t represents the total attenuation coefficient, which encompasses absorption and scattering ($\mu_t = \mu_a + \mu_s$), and d is the thickness of the sample. The same illumination sources described above were employed, however, power was measured with a photodiode power sensor (S120C, Thorlabs, Newton, NJ). Using the reduced scattering coefficient obtained from the diffuse approximation experiment, the anisotropy coefficient was calculated as $g = 1 - \mu_s'/\mu_s$.

The INO tissue-mimicking phantom was machined down to a 3x3x0.4 cm^3 slab to fulfill the thin tissue requirement. For the lymph nodes, the tissue was frozen in TissueTek OCT Compund (Sakura Finetek, Torrance, CA) and then sectioned in 100 μm thick slices using a cryostat. In order to prevent the tissue from drying, thereby affecting the optical properties, a wet cell geometry as developed by Hall *et. al*[18] was applied to mount the samples. In short, sectioned tissue was kept hydrated with phosphate buffered saline sealed between 1 mm thick glass slides and coverslips using Vaseline. While INO samples were illuminated only in the center, incident laser beams were also employed near the edge of lymph node sections. This was done to account for the variability in biological structure of the tissue and its corresponding differences in optical properties.[15]

2.3 Phantom fabrication

Epoxy resin (Castin' Craft, Fields Landing, CA) was used as the bulk material for construction of solid phantoms. This was chosen because it lends strong experimental control – the initially liquid resin permits fabrication of various shapes (determined by the mold used); and since it is transparent once cured, it allows for good manipulation of optical properties by simply adding absorbing and scattering agents. Titanium dioxide (TiO_2) powder (DuPontTM Ti-PureR, DuPont Titanium Technologies, Wilmington, DE) was used as the scattering agent as it is commonly used in

engineering and is inexpensive. To determine the amount required to mimic the optical properties of an actual lymph node, a series of 4.5x4.5x4.5 cm^3 block phantoms were formed with concentrations of TiO_2 varying from 5 mg TiO_2 /mL of resin to 13 mg TiO_2/mL in increments of 2 mg. TiO_2 powder was added to the casting resin plus 0.1% v/v ethanol to help disperse it throughout. The solution was mixed until homogeneous and then the appropriate amount of catalyst (methyl ethyl ketone peroxide) as determined by the manufacturer's instructions, was added. The solution was mixed again, ensuring no bubbles remained before pouring into silicone molds. Phantoms were left to cure for over 24h, and μ_a and μ_s' estimations were done using the method described in section 2.1. Three separate batches of each concentration were made to test for reproducibility.

3. RESULTS AND DISCUSSION

Optical properties were estimated using a two-step approach. First the absorption and reduced scattering coefficients were determined from fitting time-resolved transmittance data to the diffuse approximation to the radiative transfer equation (Eq. 1). Next, the Beer-Lambert law (Eq. 2) was applied to thin samples for estimation of the total attenuation coefficient and anisotropy factor *g*. To confirm the validity of this procedure, it was first performed on an INO phantom with known optical properties. Estimated values are listed in Table 1, and are in good agreement with the expected properties (target values provided by the manufacturer: $\mu_a = 0.05$ cm^{-1}, $\mu_s' = 10$ cm^{-1} and $g = 0.62$). Results indicated percent errors of 6.0%, 9.1%, and 2.3% for the absorption coefficient, reduced scattering coefficient, and anisotropy factor, respectively at 685 nm. Similar results were revealed for a wavelength of 780 nm (μ_a: 10%, μ_s': 6.2%, *g*: 2.6%). These findings are positive because all of the error values (with the exception of μ_s' at 685 nm) are within two sigma absolute error estimates – an accepted level of uncertainty (11.3% for μ_a and 6.8% for μ_s') deduced from a thorough error analysis study of time resolved transmittance characterization of solid phantoms.[19] It can also be noted that while the error for μ_s' at 685 nm exceeded the expected level of uncertainty (9.1% vs. 6.8%), the reported reduced scattering coefficient determined experimentally by the manufacturer for the specific batch of the phantom was also high in error (8%). Expected margins of error for *g* were not defined; however, the obtained results are consistent with what is reported in the literature ($g = 0.62 \pm 0.015$): the estimate at 685 nm falls within one standard deviation of the nominal value, and the estimate at 780 nm is within 2.6%. These results verified the reliability of the technique to characterize optical properties, thus it could be applied to lymph node tissue.

Table 1. Summary of estimated optical properties for INO phantom at 685 nm and 780 nm. Nominal optical properties $\mu_a = 0.05$ cm^{-1}, $\mu_s' = 10.0$ cm^{-1}, $g = 0.62$.

λ	μ_a (cm^{-1})	μ_s' (cm^{-1})	g
685 nm	0.053	9.094	0.634
780 nm	0.055	9.377	0.636

Representative data of time-domain signal collected from porcine lymph nodes for both wavelengths is shown below in Figure 1, and resultant lymph node optical property estimates are summarized in Table 2. Estimated absorption and reduced scattering coefficients were rather similar between wavelengths (685 nm: $\mu_a = 0.09 \pm 0.01 cm^{-1}$, $\mu_s' = 2.60 \pm 0.42$ cm^{-1}; 780 nm: $\mu_a = 0.24 \pm 0.10 cm^{-1}$, $\mu_s' = 3.35 \pm 0.14$ cm^{-1}). This can be explained based on the complex structure of lymph nodes. Although generally regarded as soft tissues, lymph nodes can exhibit fibrous and fatty tissue optical properties because they contain a fibrous capsule and perinodal adipose.[20] As such, reduced scattering coefficient values are relatively constant for these types of tissue at 685 nm and 780 nm.[14] Since the study was done in the NIR range (600-1000 nm) it was expected that scattering dominate, and that was indeed true.

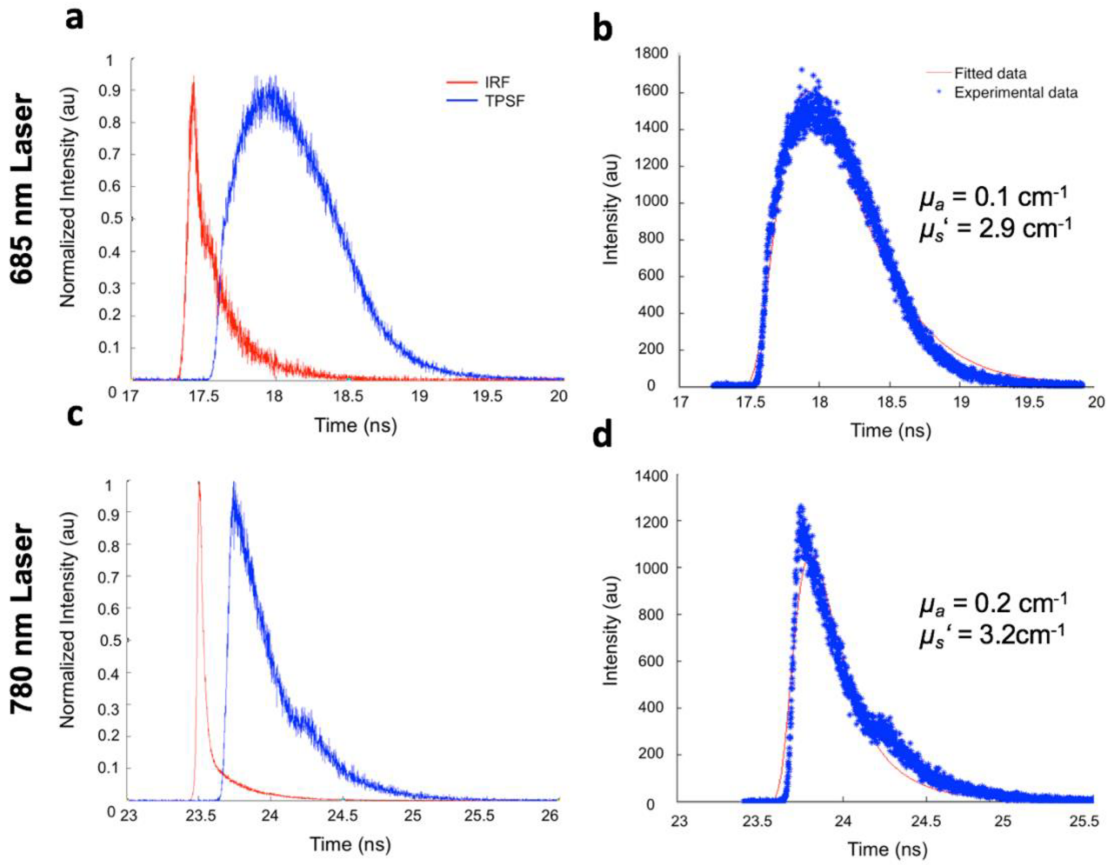

Figure 1. Time-domain signal analysis of porcine lymph node optical properties at 685 nm and 780 nm. (a,c) Sample measured instrument response functions (IRF) of the system and temporal pulse spread functions (TPSF) of the laser after passing through lymph node tissue. (b,d) Diffusion approximation model fit (red line) and measured transmittance data (blue stars).

Attenuation coefficients were obtained at the edge and center of lymph node sections to account for the variability in structure of the node tissue as stated previously. Both wavelengths revealed higher attenuation coefficients closer to the perimeter, which is expected because of the fibrous stroma encapsulating the node. These findings were consistent with trends found in the study conducted by Scolaro *et. al* where higher attenuation was observed on the periphery of human lymph nodes, and lower attenuation was found in the bulk.[15] The estimated values of μ_t are also comparable to those reported in the literature (μ_t = 45 – 153 cm^{-1} at 1320 nm). It can be noted that although the values were obtained at 1320 nm and scattering is expected to be higher at shorter wavelengths, the discrepancy may be explained by the scattering behavior of fibrous and fatty tissue, which as mentioned above also have rather constant reduced scattering coefficient values up to 1320 nm.[14] Means of μ_t = 51.1 cm^{-1} and μ_t = 43.3 cm^{-1} for 685 nm and 780 nm respectively were used to calculate anisotropy factors. Again, the obtained parameters were consistent with literature values of biological tissue (685 nm: g = 0.95, 780 nm: g = 0.95).[14]

Table 2. Summary of estimated optical properties for porcine lymph node tissue at 685 nm and 780 nm.

λ	μ_a (cm^{-1})	μ_s' (cm^{-1})	μ_t (cm^{-1})		g
			Edge	Center	
685 nm	0.09 ± 0.01	2.60 ± 0.42	57.3 ± 16.7	44.8 ± 14.5	0.95
780 nm	0.24 ± 0.10	3.35 ± 0.14	46.4 ± 17.2	40.3 ± 19.6	0.92

With μ_a, μ_s', μ_t, and g of lymph nodes defined, a physical phantom could be made to accurately mimic the optical properties of a lymph node. A series of epoxy resin block phantoms were made with increasing concentrations of TiO_2 powder to determine the required amount of scattering agent. Absorption and reduced scattering coefficients for each were estimated using the same time-resolved transmittance method applied to the lymph nodes and INO phantom. The results are shown below in Figure 2, where experimental data is plotted in red and green for 685 nm and 780 nm, respectively; and the target lymph node values ± one standard deviation are represented by the solid black line and shaded gray region, respectively. It can be seen that μ_a was relatively constant among groups for both wavelengths as expected since no absorber was added, and the coefficient underestimated the target values. Thus, future phantoms would require the addition of an absorbing agent such as India ink, which is already characterized and widely used in tissue simulating phantoms.[21] Reduced scattering coefficient estimates increased with increasing amounts of TiO_2, as anticipated. From the plots [Figs. (b) and (d)], it can be seen that a concentration on the lower end (5-7 mg TiO_2/mL) would match the desired properties of a lymph node.

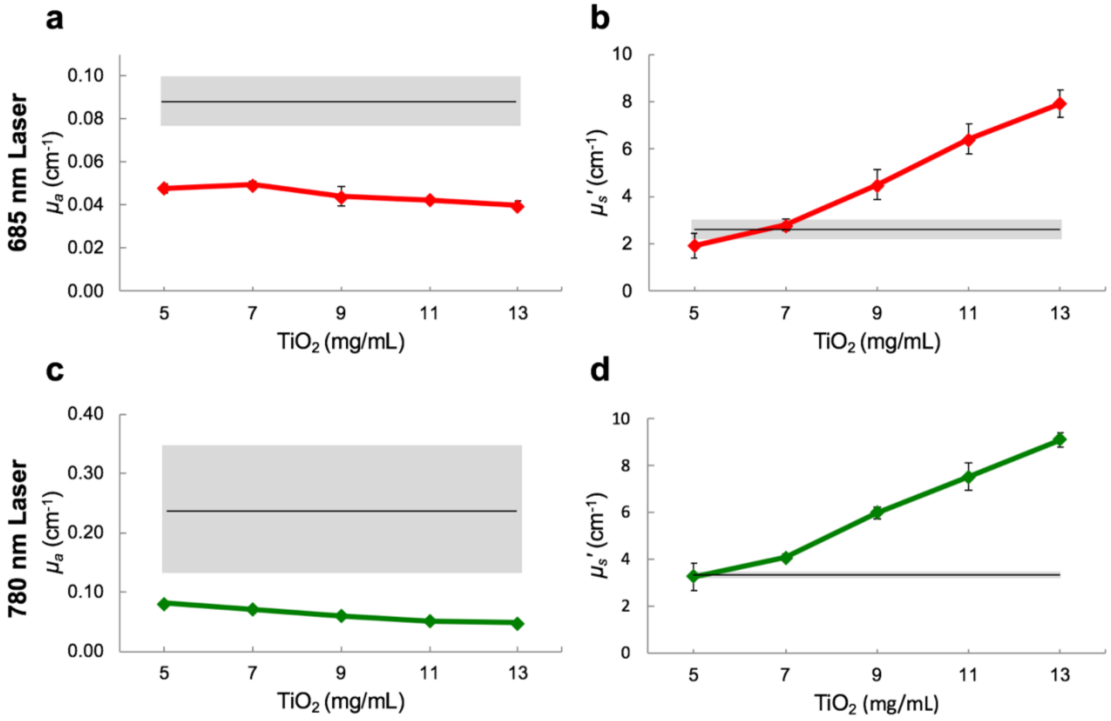

Figure 2. Estimated absorption coefficient μ_a (a,c) and reduced scattering coefficient μ_s' (b,d) of epoxy resin phantoms with increasing concentrations of scattering agent, TiO_2 at 685 nm and 780 nm. Respective target lymph node optical property values are indicated by the black solid line, and the standard deviation is represented by the shaded gray region.

4. CONCLUSION

The work presented here demonstrates a reliable method of characterizing optical properties. Measures of transmittance were applied to a diffuse model approximating the radiative transfer equation and to the Beer-Lambert law to provide estimates of μ_a, μ_s', μ_t, and g of porcine lymph nodes. The coefficients were all consistent with reported values in the literature, thus they can be used with confidence for various applications (e.g. Monte Carlo simulations, tissue-mimicking phantoms). Initial steps for creating a physical phantom with lymph node matching properties was also presented. Future work will employ these findings and verify optical imaging performance of actual lymph nodes with simulated and solid experimental phantoms using these values. With a better understanding of lymph node optical properties, limits of sensitivity, depth penetration, and resolution can be investigated; and thereby aid in the development of alternate optical imaging solutions for assessment of SLNB tissue.

REFERENCES

[1] Mehlen, P., and Puisieux, A., "Metastasis: a question of life or death," Nat Rev Cancer. 6(6),449-458, (2006).

[2] Chaffer, C.L., and Weinberg, R.A., "A Perspective on Cancer Cell Metastasis," Science. 331(6024), 1559-1564, (2011).

[3] Swartz, M. A. and Skobe, M., "Lymphatic function, lymphangiogenesis, and cancer metastasis," Microscopy research and technique. 55, 92-99, 2001.

[4] Weaver, D.L., "Pathology evaluation of sentinel lymph nodes in breast cancer: protocol recommendations and rationale," Modern pathology: an official journal of the United States and Canadian Academy of Pathology, Inc. 23 Suppl 2, S26-32, (2010).

[5] Krishnamurthy, S., Meric-Bernstam, F., Lucci, A., Hwang, R. F., Kuerer, H. M., Babiera, G., Ames, F. C., Feig, B. W., Ross, M. I., Singletary, E., Hunt, K. K. & Bedrosian, I., "A prospective study comparing touch imprint cytology, frozen section analysis, and rapid cytokeratin immunostain for intraoperative evaluation of axillary sentinel lymph nodes in breast cancer," Cancer 115, 1555-1562, (2009).

[6] Tsujimoto, M., Nakabayashi, K., Yoshidome, K., Kaneko, T., Iwase, T., Akiyama, F., Kato, Y., Tsuda, H., Ueda, S., Sato, K., Tamaki, Y., Noguchi, S., Kataoka, T. R., Nakajima, H., Komoike, Y., Inaji, H., Tsugawa, K., Suzuki, K., Nakamura, S., Daitoh, M., Otomo, Y. and Matsuura, N., "One-step nucleic acid amplification for intraoperative detection of lymph node metastasis in breast cancer patients," Clinical cancer research : an official journal of the American Association for Cancer Research. 13, 4807-4816, (2007).

[7] Hartana, C. A., Kinn, J., Rosenblatt, R., Anania, S., Alamdari, F., Glise, H., Sherif, A. & Winqvist, O. "Detection of micrometastases by flow cytometry in sentinel lymph nodes from patients with renal tumours," British journal of cancer 115, 957-966, (2016).

[8] Li, C., Torres, V.C., and Tichauer, K.M., "Noninvasive detection of cancer spread to lymph nodes: A review of molecular imaging principles and protocols," J Surg Oncol. 1-14 (2018).

[9] Ntziachristos, V., "Going deeper than microscopy: the optical imaging frontier in biology," Nat Methods **7**, 603-614 (2010).

[10] Sinha, L., Massanes, F., Torres, V.C., Li, C., Tichauer, K.M., and Brankov, J.G., "Comparison of early-photon and angular-domain scatter rejection in mesoscopic optical imaging: a simulation study," Manuscript submitted for publication.

[11] Tang, Q., Liu, Y., Tsytsarev, V., Lin, J., Wang, B., Kanniyappan, U., Li, Z., and Chen, Y., "High-dynamic-range fluorescence laminar optical tomography (HDR-FLOT)," Biomed Opt Exp 8, 2124-2137 (2017).

[12] Ozturk, M.S., Lee, V.M., Zhao, L., Dai, G., and Intes, X., "Mesoscopic fluorescence molecular tomography of reporter genes in bioprinted thick tissue," J Biomed Opt. 18, 100501(2013).

[13] Anastasopoulou, M., Koch, M., Gorpas, D., Karlas, A., Klemm, U., Garcia-Allende, P.B., and Ntziachristos, V., "Comprehensive phantom for interventional fluorescence molecular imaging," J Biomed Opt. 21(9), 091309 (2016).

[14] Jacques, S. L., "Optical properties of biological tissues: a review," Phys Med Bio. 58, R37-61 (2013).

[15] Scolaro, L., McLaughlin, R. A., Klyen, B. R., Wood, B. A., Robbins, P. D., Saunders, C. M., Jacques, S. L. and Sampson, D. D., "Parametric imaging of the local attenuation coefficient in human axillary lymph nodes assessed using optical coherence tomography," Biomedical optics express. 3, 366-379 (2012).

[16] Patterson, M. S., Chance, B., and Wilson, B. C., "Time resolved reflectance and transmittance for the non-invasive measurement of tissue optical properties," Applied optics 28, 2331-2336 (1989).

[17] Sinha, L., Fogarty, M., Zhou, W., Giudice, A., Brankov, J. G., and Tichauer, K. M., "Design and characterization of a dead-time regime enhanced early photon projection imaging system," Rev Sci Instrum. 89, 043707 (2018).

[18] Hall, G., Jacques, S. L., Eliceiri, K. W., and Campagnola, P. J., "Goniometric measurements of thick tissue using Monte Carlo simulations to obtain the single scattering anisotropy coefficient," Biomedical optics express. 3, 2707-2719 (2012).

[19] Bouchard, J. P., Veilleux, I, Jedidi, R., Noiseux, I., Fortin, M., and Mermut, O., "Reference optical phantoms for diffuse optical spectroscopy. Part 1--Error analysis of a time resolved transmittance characterization method," Opt Express. 18, 11495-11507 (2010).

[20] Willard-Mack, Cynthia L. "Normal Structure, Function, and Histology of Lymph Nodes," Toxicologic Pathology. 34(5), 409–424 (2006).

[21] Di Ninni, P., Martelli, F., and Zaccanti, G., "The use of India ink in tissue-simulating phantoms," Optics Express. 18(26), 26854-26865 (2010).